

RESEARCH LETTER

10.1002/2017GL073528

Key Points:

- Depth extent and integrity of the subducting Indian plate beneath the Indochina Peninsula are revealed by this receiver function MTZ study
- Independent evidence is obtained for the presence of slab segments in the MTZ beneath central and a slab window beneath western peninsula
- Mantle upwelling induced by sinking of the broken-off slab segments may have led to volcanic centers and mantle LVZ east of the Peninsula

Supporting Information:

- Supporting Information S1

Correspondence to:

Y. Yu,
yuyouqiang@tongji.edu.cn

Citation:

Yu, Y., S. S. Gao, K. H. Liu, T. Yang, M. Xue, and K. Phon Le (2017), Mantle transition zone discontinuities beneath the Indochina Peninsula: Implications for slab subduction and mantle upwelling, *Geophys. Res. Lett.*, *44*, 7159–7167, doi:10.1002/2017GL073528.

Received 19 MAR 2017

Accepted 24 MAY 2017

Accepted article online 30 MAY 2017

Published online 19 JUL 2017

Mantle transition zone discontinuities beneath the Indochina Peninsula: Implications for slab subduction and mantle upwelling

Youqiang Yu¹ , Stephen S. Gao² , Kelly H. Liu² , Ting Yang³, Mei Xue¹ , and Khanh Phon Le⁴

¹State Key Laboratory of Marine Geology, Tongji University, Shanghai, China, ²Geology and Geophysics Program, Missouri University of Science and Technology, Rolla, Missouri, USA, ³School of Oceanography, Southern University of Science and Technology, China, ⁴Faculty of Oil and Gas, Hanoi University of Mining and Geology, Hanoi, Vietnam

Abstract While the northward indentation of the Indian into Eurasian plates has been intensively investigated, its oblique subduction beneath the Indochina Peninsula (ICP) and the role it played on mantle structure and dynamics remain enigmatic. In this first regional-scale receiver function study of the mantle transition zone (MTZ) discontinuities beneath the ICP and its surrounding areas, we stack ~12,000 receiver functions recorded at 33 stations using a non-plane wave common-conversion-point stacking technique. Systematic spatial variations of MTZ thickness with departures between –21 and +24 km from the globally averaged value are revealed, providing independent evidence for the presence of slab segments in the MTZ beneath the central and a slab window beneath the western ICP. The results also support the existence of broad mantle upwelling adjacent to the eastern edge of the slab segments, which might be responsible for the widespread Cenozoic volcanisms and pervasively observed upper mantle low velocities in the area.

1. Introduction

The collision between the Indian and Eurasian plates over the past 50 Ma not only created the Himalayan-Tibetan orogen but also dramatically influenced the Cenozoic tectonic evolution of Southeast Asia [e.g., *Tapponnier et al.*, 1982; *Avouac and Tapponnier*, 1993]. Situated above the mantle wedge of the obliquely subducting Indian Plate beneath the Eurasian and Sunda plates, the Indochina Peninsula (ICP), which is the largest landmass of Southeast Asia and is mainly composed of the Shan-Thai and Indochina Blocks (Figure 1), has experienced extrusion of at least 500 km and clockwise rotation since 35 Ma [e.g., *Tapponnier et al.*, 1986; *Leloup et al.*, 1995; *Steckler et al.*, 2016]. In contrast to typical subduction zones where the Wadati-Benioff zone extends to the bottom of the upper mantle or even the mantle transition zone, all the magnitude ≥ 4.0 earthquakes occurred beneath the ICP between 1980 and 2016 are shallower than 200 km (Figure 1, inset).

While most seismic tomography studies reveal slower-than-normal upper mantle velocities beneath most part of the ICP [*Li et al.*, 2008; *Pesicek et al.*, 2008, 2010; *Z. Huang et al.*, 2015; *Yang et al.*, 2015], inconsistent results have been reported regarding the depth, lateral extent, and integrity of the aseismic sections of the subducted Indian Plate. Consequently, the possible roles that the subduction played on the generation of the slow upper mantle seismic velocities and the widespread Cenozoic volcanisms found along the eastern margin of the ICP (Figure 1) remain controversial. For instance, while some teleseismic tomography studies show evidence for the presence of the subducted Indian slab sinking into the mantle transition zone (MTZ) under the ICP [*Li et al.*, 2008; *Pesicek et al.*, 2008; *Li and van der Hilst*, 2010; *Pesicek et al.*, 2010], the higher-velocity anomalies in the MTZ beneath the ICP are not clearly revealed in some more recent and presumably higher-resolution studies [e.g., *Z. Huang et al.*, 2015]. Similarly, whether the slab subducts as a single piece or has broken into segments in the upper mantle and MTZ is also an unresolved issue [*Pesicek et al.*, 2008, 2010]. Those uncertainties are most likely the results of an unfortunate combination of the paucity of available seismic data in the area and the intrinsic limitation of the resolving power of the seismic tomography techniques [*Foulger et al.*, 2013].

Independent constraints on the thermal and velocity structure of the Earth's upper mantle and MTZ can be obtained by seismologically imaging the 410 km and 660 km discontinuities (hereafter referred to as d_{410} and d_{660}), which define the top and bottom of the MTZ [*Shearer and Flanagan*, 1999]. The d_{410} and d_{660} represent phase transitions from olivine to wadsleyite (β spinel) and from ringwoodite (γ spinel) to bridgmanite

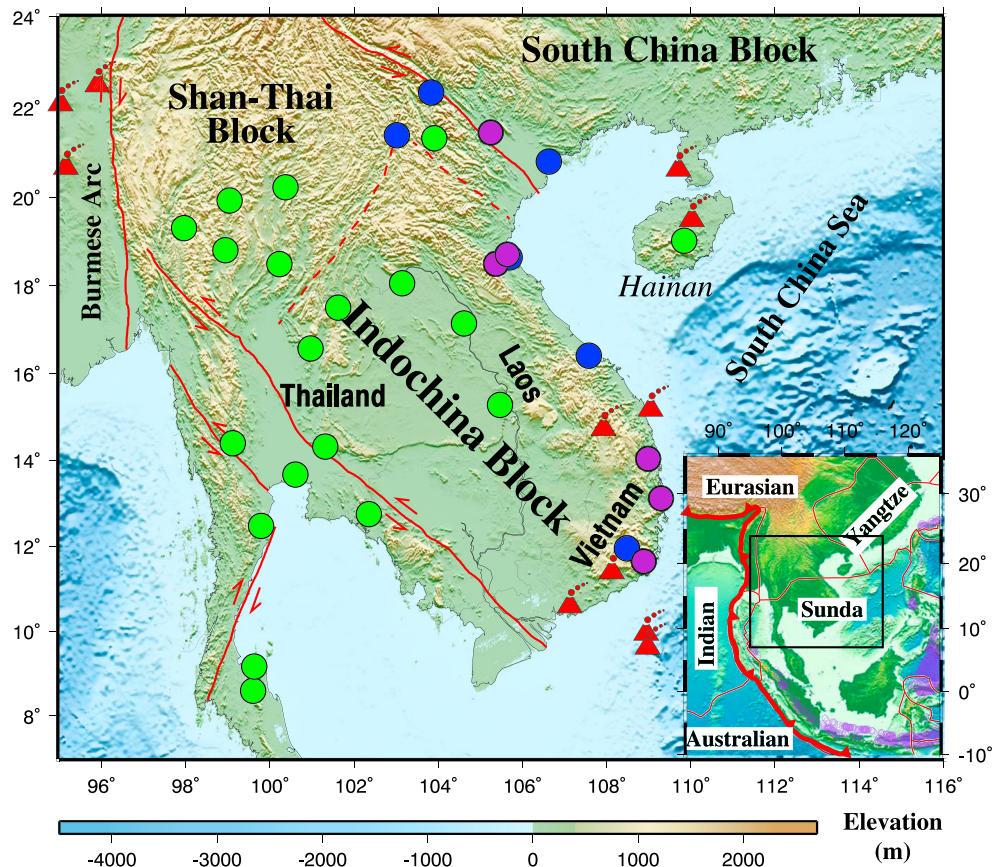


Figure 1. Topographic map showing the distribution of seismic stations and major tectonic features of the study area. Green, purple, and blue circles represent stations from IRIS, Tongji University, and the University of Tokyo, respectively. Red solid and dashed lines are major faults and sutures modified from *Leloup et al. [1995]* and *Takemoto et al. [2009]*. The red triangular symbols are Cenozoic volcanoes. The inset shows the location of the study area highlighted by the black rectangle. The thick red line represents the trench, and the thin red lines are plate boundaries based on *Bird [2003]*. Purple circles are magnitude ≥ 4.0 earthquakes occurred from 1980 to 2016 with a focal depth ≥ 200 km.

and ferropericlase, respectively [*Ringwood, 1975; Tschauner et al., 2014*]. Although reported magnitude of the Clapeyron slopes associated with the phase transitions varies among different studies, it has been demonstrated by numerous investigations that the transition occurring at the $d410$ has a positive Clapeyron slope (e.g., 2.9 MPa/K in *Bina and Helffrich [1994]*) and that at the $d660$ has a negative value (e.g., -1.3 MPa/K in *Fei et al. [2004]*), indicating that thermal anomalies such as those caused by subducted cold slabs and hot mantle upwelling can lead to thicker and thinner MTZ, respectively. The existence of hydrous minerals in the MTZ has similar effects as low temperatures and would thicken the MTZ [*Litasov et al., 2005*]. Therefore, variations of the depths of the $d410$ and $d660$ are in situ indicators of the thermal state and water content of the MTZ and can provide independent constraints on the existence and spatial distribution of subducted slabs and mantle upwellings in the vicinity of the discontinuities [*Ringwood, 1975; Bina and Helffrich, 1994*].

Previous MTZ studies in Southeast Asia are mostly restricted in the Hainan Island region located in the north-eastern part of the study area (Figure 1). Most studies [*Wang and Huang, 2012; H. Huang et al., 2015; Wei and Chen, 2016*] reveal an MTZ of about 25 km thinner than the normal value of 250 km in the IASP91 and most other earth models, which is attributed to a mantle plume originating from the lower mantle. The MTZ beneath the vast majority of the ICP has not been investigated. In this study, we present results from the first receiver function (RF) study of the MTZ beneath the entirety of the ICP and adjacent areas based on a non-plane wave common-conversion-point stacking procedure [*Gao and Liu, 2014a*]. Our results provide evidence for the existence of a slab window beneath the western ICP, slab segments beneath the central part, and thermal upwelling beneath the area adjacent to the slab segments that might be responsible for the generation of Cenozoic volcanism and slow upper mantle velocities found along a zone east of the peninsula.

2. Data and Method

Three-component broadband data used in this study were recorded by a total of 33 stations and were obtained from three sources, including (1) 21 stations mainly distributed in Thailand, data from which are publicly available through the Incorporated Research Institutions for Seismology (IRIS) Data Management Center (DMC) for the recording period of 2009 to 2016; (2) 6 stations in a temporary network deployed in Vietnam by the University of Tokyo from early 2000 to late 2005 [Bai *et al.*, 2009, 2010]; and (3) another 6 portable stations deployed in Vietnam by the Seismological Group at Tongji University for the period of 2009–2012 [Yang *et al.*, 2015]. Teleseismic events with an epicentral distance in the range of 30–100° are selected using a cutoff magnitude for data requesting determined using an empirical formula reliant upon epicentral distance and event focal depth, in order to balance the quantity and quality of the seismic data to be requested [Liu and Gao, 2010].

Detailed descriptions of the data processing and selection procedure and criteria can be found in Gao and Liu [2014b] for a study of MTZ discontinuities beneath the contiguous United States and are briefly summarized below. The requested seismograms are windowed 20 s before and 260 s after the theoretical *P* arrival time computed using the IASP91 Earth model and are band pass filtered with a four-pole and two-pass Bessel filter in the frequency band of 0.02–0.2 Hz. We then apply a set of exponential functions centered on the theoretical *PP* arrival, which has a strong amplitude and a different ray parameter relative to the first arrival, to reduce its degenerating effects to the resulting RFs [Gao and Liu, 2014a]. The corrected seismograms with signal-to-noise ratios (SNR) above 4.0 on the vertical component are employed to generate the RFs by deconvolving the vertical from the radial components following the frequency-domain water level deconvolution procedure [Langston, 1979; Ammon, 1991]. The resulting RFs with strong noise before the *P* arrival or abnormal arrivals in the *P* wave coda are rejected using an SNR-based procedure. A total of 12,065 high-quality RFs from 4906 teleseismic events are obtained. The *P*-to-*S* arrivals from the *d*410 and *d*660 are clearly observed when plotted against the epicentral distance and follow the theoretical moveout curves well (Figure S1 in the supporting information). To our knowledge, this is the first regional-scale RF study aiming at imaging the MTZ beneath the whole ICP.

The study area is evenly divided into overlapping circular bins with a radius of 1°, which is approximately the size of the first Fresnel zone of shear waves at the MTZ depth, and with a distance of one geographic degree between the center of neighboring bins. RFs with ray piercing points (computed at the middle of the MTZ) within the same bins are moveout corrected based on the IASP91 Earth model and are stacked to form depth series under the non-plane wave assumption [Gao and Liu, 2014a]. Such a common-conversion-point procedure considers the fact that the ray parameters for the direct *P* wave and the converted *S* wave are different and thus can more accurately determine the discontinuity depths and improve the stacking amplitude of the *P*-to-*S* arrivals from the discontinuities.

Bins with less than eight RFs are rejected to minimize the possibility of misidentifying the arrivals from the targeted discontinuities. The mean and standard deviation of the MTZ discontinuity depths are obtained by applying a bootstrap resampling approach with 50 iterations [Efron and Tibshirani, 1986]. Note that as the 1-D IASP91 Earth model is utilized for moveout correction and time-depth conversion, the resulting discontinuity depths are apparent rather than true depths. To obtain the true depths (e.g., as demonstrated in Gao and Liu [2014b] for the contiguous United States), well-determined V_p and V_s velocity models with sufficient spatial resolution covering the entire upper mantle and MTZ are needed. Unfortunately, such velocity models are not available in our study area, and thus, in the following the apparent depths will be used. As evidenced below and by the vast majority of MTZ studies, which used 1-D models for the time-depth conversion, the apparent depths and MTZ thickness can provide valuable information about the thermal structure of both the upper mantle and MTZ.

3. Results

The resulting depth series from each bin were visually examined to reject those with weak arrivals or ambiguous peaks in the anticipated depth ranges of the MTZ discontinuities. All the 172 bins with at least one of the two MTZ discontinuities are shown in Figure 2 along the 16 latitudinal profiles, among which 161 bins possess reliable *d*410 peaks, 143 demonstrate clearly observable *d*660 arrivals, and 132 have both from which MTZ thickness can be measured. The number of RFs used for moveout correction and stacking of each bin ranges

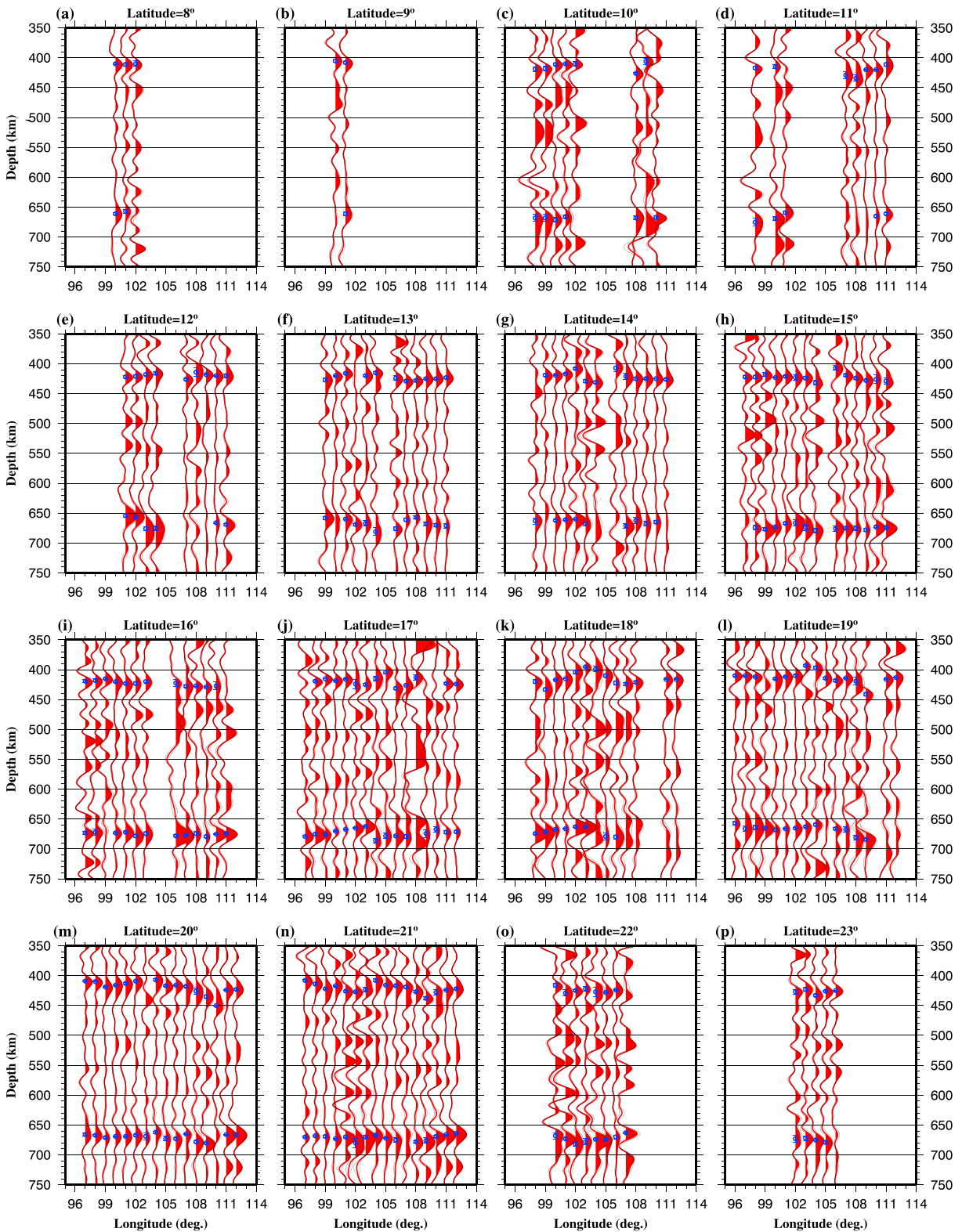


Figure 2. Results of stacking moveout-corrected RFs within each bin plotted along 16 latitudinal profiles. For each bin, the thick red line shows the mean depth series averaged over the bootstrap iterations, and the bordering thin black lines indicate the mean \pm standard deviations. The circles and error bars represent the resulting apparent depths and standard deviations of the depths of the MTZ discontinuities.

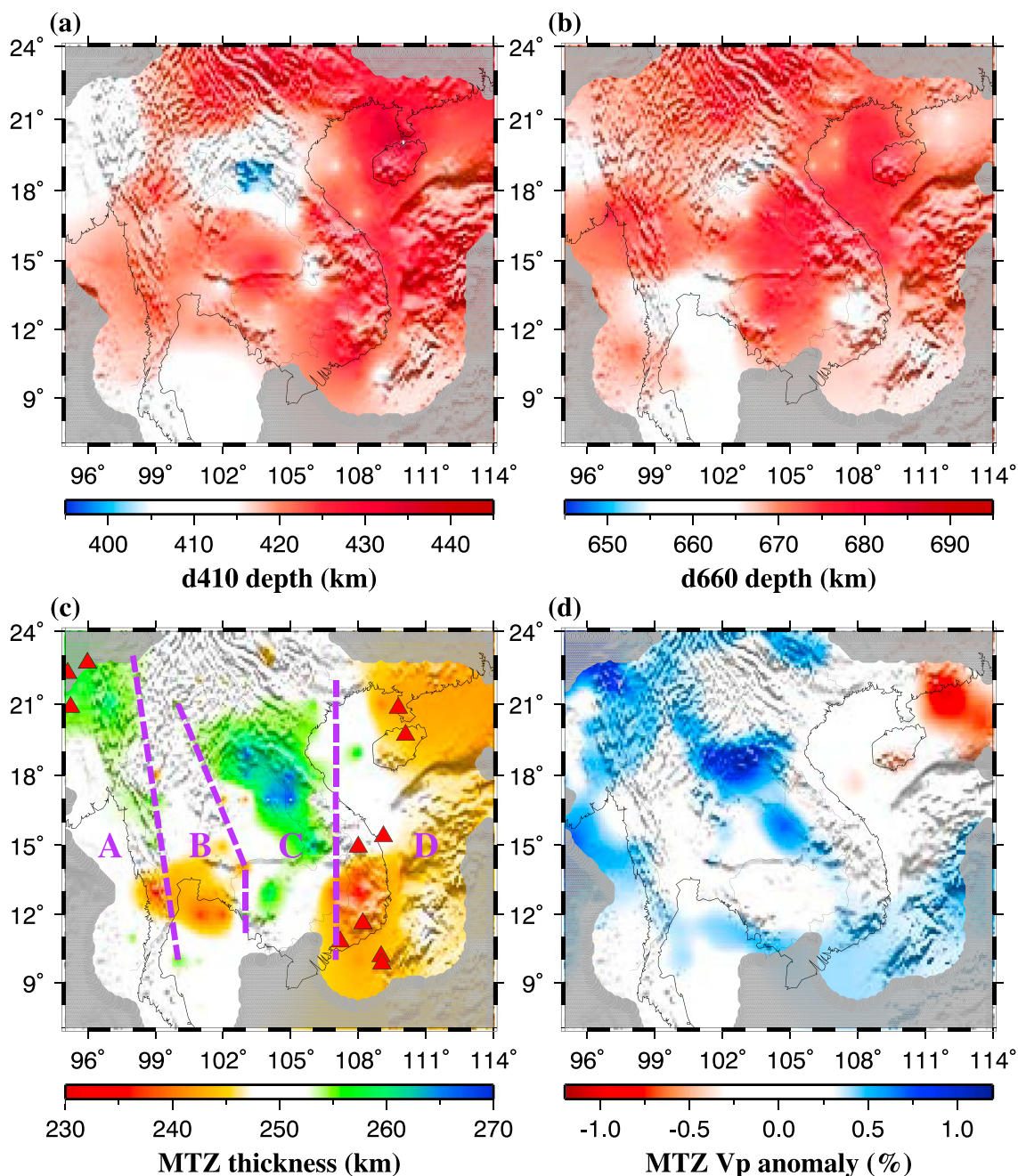


Figure 3. (a) Spatial distribution of the resulting apparent depths the d_{410} . (b) Same as Figure 3a but for the d_{660} . (c) Resulting MTZ thicknesses. The red triangles indicate Cenozoic volcanic centers, and the purple dashed lines divide the area into four regions based on observed characteristics of MTZ discontinuities. Region A is occupied by the subducting Indian slab, Region B contains a slab window, Region C contains slab fragments in the MTZ, and Region D is dominated by thermal upwelling. (d) Average P wave velocity anomaly in the MTZ calculated from the tomography model of Li and van der Hilst [2010].

from 8 to 2621 with a mean of 225. The robustness of the d_{410} and d_{660} arrivals is most clearly demonstrated when the stacked depth series are arranged according to the apparent depth of the d_{410} (Figure S2b) and that of d_{660} (Figure S2c).

To the first order, the resulting apparent depths of the d_{410} and d_{660} are generally deeper than the theoretical values of 410 km and 660 km in the IASP91 Earth model, with an average of 419.4 ± 8.4 km and 670.0 ± 6.4 km, respectively (Figure 3), while the MTZ has a normal thickness of 250.0 ± 8.0 km. The d_{410} is the shallowest (393 km) in the central part of the study area, and the maximum d_{410} depth of 450 km is found beneath the Hainan area. The depth of the d_{660} ranges from 654 km beneath the southwestern part of the Indochina

Block to 686 km around the middle coastal area of Vietnam. The cross-correlation coefficient (XCC) between the apparent depths of the d_{410} and d_{660} is about 0.39. In comparison, the XCC for the contiguous United States is as high as 0.84 [Gao and Liu, 2014b]. The lower XCC suggests that relative to the latter area, the upper mantle velocities, which affect the apparent depths of both discontinuities, are less heterogeneous beneath the study area. Similarly, it may also indicate stronger lateral velocity variations in the MTZ, which only affect the apparent depths of the d_{660} .

Significant lateral variations of the MTZ thicknesses are revealed, ranging from 229 km beneath Hainan to 274 km beneath the central ICP, i.e., -21 to $+24$ km from the global mean of 250 km. The central and western parts of the ICP are predominantly characterized by a thicker-than-normal MTZ, the southwestern and especially eastern edges of the Peninsula are dominated by a thinner-than-normal MTZ, while the rest of the area possess mostly normal (within ± 2.5 km) MTZ thickness (Figure 3c).

4. Discussion

The systematic spatial distribution of the apparent depths of the d_{410} and d_{660} and the MTZ thickness provides constraints on a number of important and previously unresolved issues related to the subducted Indian slab and its influence on the Cenozoic tectonic development of the ICP.

4.1. Slab Segments in the MTZ

Beneath the ICP, an outstanding spatial correspondence is found between the area with the thickest MTZ (Figure 3c) and the area with the highest P wave velocity anomaly in the MTZ revealed by Li and van der Hilst [2010] (Figure 3d). Specifically, the NW-SE trending zone in the central part of the study area possesses an MTZ that is up to 24 km thicker than the normal value of 250 km, as well as a prominent V_p anomaly of about $+1\%$. If we use a scaling parameter of $dV_p/dT = -4.8 \times 10^{-4} \text{ km s}^{-1} \text{ K}^{-1}$ [Deal et al., 1999], the corresponding temperature anomaly is about -200 K. For a Clapeyron slope of $+2.9$ MPa/K for the d_{410} [Bina and Helffrich, 1994] and -1.3 MPa/K for the d_{660} [Fei et al., 2004], the temperature anomaly leads to an MTZ thickening of 24 km which is perfectly consistent with the observed magnitude of the thickening. Because the high-velocity anomalies disappear in the layers below the MTZ [Li and van der Hilst, 2010], the simplest explanation of the above observation is that the slab segments are deflected horizontally in the MTZ and have not penetrated into the lower mantle (Figure 4). The spatial distribution of the MTZ thickness measurements is consistent with some of the seismic tomography studies [e.g., Li et al., 2008; Pesicek et al., 2008; Li and van der Hilst, 2010; Pesicek et al., 2010] but is inconsistent with others that did not reveal high-velocity anomalies in the MTZ [e.g., Huang and Zhao, 2006; Z. Huang et al., 2015].

In principle, the thickening of the MTZ observed in Area C (Figure 4) can also be caused by the presence of water [e.g., Litasov et al., 2005]. However, some previous studies have suggested that under normal pressure-temperature conditions, water can lead to a low-velocity anomaly and broaden the interval of the phase transition associated with the d_{410} , leading to anomalously low stacking amplitude [Wood, 1995]. Both predicted anomalies are not observed. Instead, seismic tomography studies have revealed a high-velocity zone corresponding to the zone of thickened MTZ [Li and van der Hilst, 2010], and no anomalies in the stacking amplitudes are observed in this zone (Figure 2). Thus, the amount of water in the MTZ beneath the study area is probably minor.

4.2. A Slab Window Beneath the Western ICP

Some seismic tomography studies suggest that the eastward subducting Indian slab has broken off and left a slab window beneath the western ICP [Pesicek et al., 2008], while others find it to be a continuous feature [Pesicek et al., 2010]. The existence of a slab window is in line with geochronological and geochemical studies, which have proposed a mechanism of upwelling asthenosphere induced by a break-off slab to explain the mafic and intermediate dykes observed in the western margin of the Indochina Block [e.g., Arboit et al., 2016].

A slab window can explain the apparent normal and slightly thinner-than-normal MTZ thicknesses in Area B, which is the area between the two areas with thicker-than-normal MTZ located in the western and central parts of the study area (Areas A and C, respectively; Figure 3c). It might also be responsible for the hotter-than-normal upper mantle velocities revealed by seismic tomography studies [Li and van der Hilst, 2010] as indicated by the apparent depression of both the d_{410} and d_{660} (Figures 3a and 3b) that are found in Area B (Figure 3c). In addition, in the area where the slab window is suggested, the d_{410} has a greater apparent depression than the d_{660} , which can be more clearly observed in the westernmost three traces

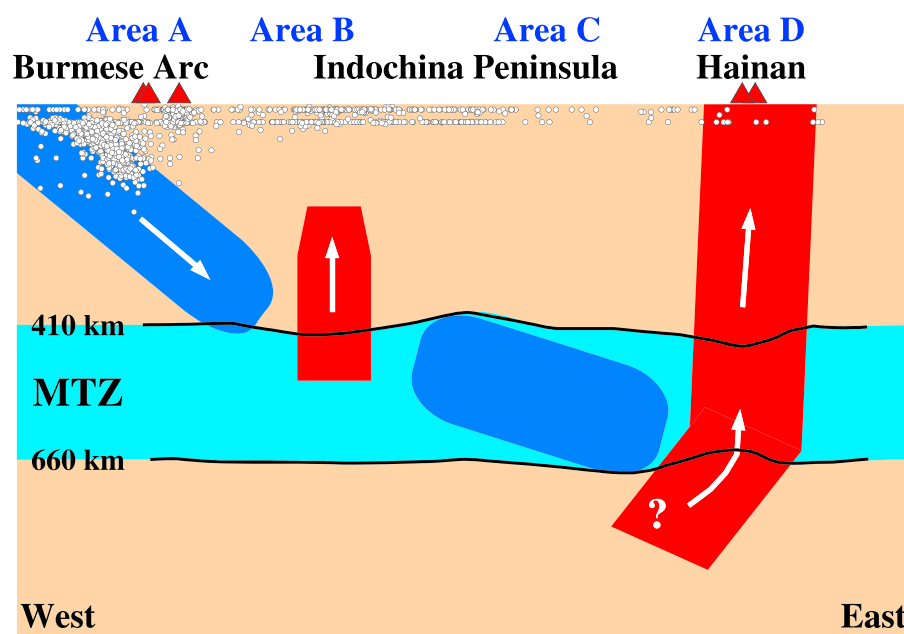


Figure 4. A schematic diagram showing the major features of the upper mantle structure and dynamic processes beneath the ICP and surrounding areas constructed based on our observations and previous seismic tomography results from Pesicek *et al.* [2008], Li and van der Hilst [2010], and Huang [2014]. The dark blue bodies are slab segments, the red columns represent thermal upwelling, triangles indicate volcanoes, and the open dots show the earthquakes.

in Figure 2k. This feature can be the result of the upwelling of hotter material from the MTZ to the upper mantle through the slab window (Figure 4). A numerical simulation study suggests that this upwelling is part of a return flow system induced by actively sinking slab segments and is capable of producing decompression melting in the upper mantle [Faccenna *et al.*, 2010]. A similar mechanism is involved in a recent RF study to explain low upper mantle velocities and Cenozoic volcanism in southwestern China, directly to the north of our study area [Zhang *et al.*, 2017].

4.3. Thermal Upwelling Adjacent to Slab Segments in the MTZ

An approximately N-S elongated zone of thinner-than-normal MTZ is revealed to the east of the ICP, adjacent to the slab segments inferred from the thick MTZ and high MTZ velocities (Figure 3c). This zone is also home to pervasive Cenozoic volcanisms (Figure 3c) and is characterized by an apparent depression of the d_{410} of about 15–20 km (Figure 3a). If we assume that the true depth of the d_{410} is 410 km, the apparent depression suggests an overall lower-than-normal upper mantle and crustal velocities with magnitude of -1.1% to -1.5% [Gao and Liu, 2014a], a value that is comparable to results from seismic tomography investigations [e.g., Montelli *et al.*, 2004; Li *et al.*, 2008, 2009; Wang and Huang, 2012; Le *et al.*, 2015; Xia *et al.*, 2016]. The maximum MTZ thinning of 21 km is found beneath southern Vietnam, corresponding to a thermal anomaly of about +180 K. The amount of thinning in the Hainan area is about 15 km, which is similar to those reported in previous studies covering this area [Wang and Huang, 2012; Huang, 2014; H. Huang *et al.*, 2015; Wei and Chen, 2016].

Isotopic studies of basalts in the Hainan area suggest a source depth in the MTZ or possibly lower mantle [Zou and Fan, 2010]. However, investigations on petrogenesis of Cenozoic basalts from Vietnam favor a model with mantle upwelling induced by decompression melting in the shallow upper mantle [Hoang and Flower, 1998; Hoang *et al.*, 2013]. In general, most of the geochemical studies are not supportive of a classic plume from the lower mantle as the source of the volcanoes [e.g., Hoang and Flower, 1998; Hoang *et al.*, 2013].

Three main observations, including the thinner-than-normal MTZ observed beneath the area east of the ICP, its immediate proximity with the inferred eastward extension of slab segments in the MTZ, and previously revealed lateral and vertical distribution of low-velocity anomalies in the upper mantle and MTZ, support a model of slab-induced thermal upwelling probably originating from beneath the slab (Figure 4). This model postulates that sinking of the slab segments deflects underlying mantle flow and induces thermal upwelling

through the MTZ and upper mantle, giving rise to a zone of high temperature that results in the observed thin MTZ. Continuous upwelling of the hot material in the upper mantle led to low seismic velocities and ultimately resulted in volcanism observed above the zone of thin MTZ. The mechanism of such upwelling is similar to subduction-triggered magmatic pulses observed in the back-arc region and around the edges of the slab, as indicated by geodynamic modeling [Faccenna *et al.*, 2010]. Similarly, basaltic magmatism observed above slab segments beneath Yellowstone [James *et al.*, 2011] and NE China [Tang *et al.*, 2014] has been attributed to slab-induced thermal upwelling.

5. Conclusions

This first regional-scale receiver function investigation of mantle transition zone discontinuities beneath the Indochina Peninsula and surrounding areas provides clear evidence for the presence of slab segments in the MTZ beneath the central part of the peninsula. The slabs produce a temperature anomaly up to -200 K which results in a thickening of the MTZ by about 24 km. Hotter-than-normal upper mantle temperature and a gap in MTZ thickening are found beneath the western part of the peninsula and may correspond to a previously proposed slab window that separates the broken-off slab segments in the MTZ and the subducting younger section of the Indian slab. Sinking of the broken-off segments may have deflected underlying mantle flow and led to its upward movement, which in turn might be responsible for the observed up to 21 km thinning of the MTZ and low upper mantle seismic velocities revealed beneath a zone adjacent to the eastern edge of the slab segments. This study clarifies a number of long-standing controversies regarding the geometry and integrity of the Indian slab beneath the Indochina Peninsula and proposes a mechanism for the formation of the low upper mantle velocities and Cenozoic volcanisms pervasively observed to the east of the Peninsula. The subduction of the Indian slab beneath the Indochina Peninsula strongly influenced mantle structure and dynamics as well as Cenozoic tectonic features such as volcanisms observed on the surface.

Acknowledgments

Data from the 21 permanent stations were obtained from the IRIS DMC (last accessed: May 2016). We thank the Earthquake Research Institute, the University of Tokyo, for sharing the Vietnam array data (which can be accessed from <http://ohpdm.eri.u-tokyo.ac.jp/>). Data from the six-station portable network in Vietnam were collected and archived by the Seismology Group at Tongji University and are available upon request. Comments from two anonymous reviewers greatly improved the manuscript. This study is funded by the National Natural Science Foundation of China through grants 41606043 and 41676033 and the National Program on Global Changing and Air-Sea Interaction (grant GASI-GEOGE-05).

References

- Ammon, C. J. (1991), The isolation of receiver effects from teleseismic *P*-waveforms, *Bull. Seismol. Soc. Am.*, *81*, 2504–2510.
- Arboit, F., A. S. Collins, C. K. Morley, F. Jourdan, R. King, J. Foden, and K. Amrouch (2016), Geochronological and geochemical studies of mafic and intermediate dykes from the Khao Khwang Fold-Thrust Belt: Implications for petrogenesis and tectonic evolution, *Gondwana Res.*, *36*, 124–141, doi:10.1016/j.gr.2016.04.005.
- Avouac, J.-P., and P. Tapponnier (1993), Kinematic model of active deformation in central Asia, *Geophys. Res. Lett.*, *20*(10), 895–898, doi:10.1029/93GL00128.
- Bai, L., T. Iidaka, H. Kawakatsu, Y. Morita, and N. Q. Dzong (2009), Upper mantle anisotropy beneath Indochina block and adjacent regions from shear-wave splitting analysis of Vietnam broadband seismograph array data, *Phys. Earth Planet. Inter.*, *176*(1), 33–43, doi:10.1016/j.pepi.2009.03.008.
- Bai, L., X. Tian, and J. Ritsema (2010), Crustal structure beneath the Indochina Peninsula from teleseismic receiver functions, *Geophys. Res. Lett.*, *37*, L24308, doi:10.1029/2010GL044874.
- Bina, C. R., and G. Helffrich (1994), Phase transition Clapeyron slopes and transition zone seismic discontinuity topography, *J. Geophys. Res.*, *99*(B8), 15853–15860, doi:10.1029/94JB00462.
- Bird, P. (2003), An updated digital model of plate boundaries, *Geochem. Geophys. Geosyst.*, *4*, 1027, doi:10.1029/2001GC000252.
- Deal, M. M., G. Nolet, and R. D. van der Hilst (1999), Slab temperature and thickness from seismic tomography: 1. Method and application to Tonga, *J. Geophys. Res.*, *104*(B12), 28,789–28,802, doi:10.1029/1999JB900255.
- Efron, B., and R. Tibshirani (1986), Bootstrap methods for standard errors, confidence intervals, and other measures of statistical accuracy, *Stat. Sci.*, *1*, 54–75.
- Faccenna, C., T. W. Becker, S. Lallenmand, Y. Lagabrielle, F. Funicello, and C. Piromallo (2010), Subduction-triggered magmatic pulses: A new class of plumes?, *Earth Planet. Sci. Lett.*, *299*, 54–68, doi:10.1016/j.epsl.2010.08.012.
- Fei, Y., J. Van Orman, J. Li, W. van Westrenen, C. Sanloup, W. Minarik, K. Hirose, T. Komabayashi, M. Walter, and K. Funakoshi (2004), Experimentally determined postspinel transformation boundary in Mg_2SiO_4 using MgO as an internal pressure standard and its geophysical implications, *J. Geophys. Res.*, *109*, B02305, doi:10.1029/2003JB002562.
- Foulger, G. R., et al. (2013), Caveats on tomographic images, *Terra Nova*, *25*, 259–281, doi:10.1111/ter.12041.
- Gao, S. S., and K. H. Liu (2014a), Imaging mantle discontinuities using multiply-reflected *P*-to-*S* conversions, *Earth Planet. Sci. Lett.*, *402*, 99–106, doi:10.1016/j.epsl.2013.08.025.
- Gao, S. S., and K. H. Liu (2014b), Mantle transition zone discontinuities beneath the contiguous United States, *J. Geophys. Res. Solid Earth*, *119*, 6452–6468, doi:10.1002/2014JB011253.
- Hoang, N., and M. Flower (1998), Petrogenesis of Cenozoic basalts from Vietnam: Implications for origin of a “diffuse igneous province”, *J. Petrol.*, *39*, 369–395, doi:10.1093/ptroj/39.3.369.
- Hoang, N., M. F. Flower, C. T. Chi, P. T. Xuan, H. V. Quy, and T. T. Son (2013), Collision-induced basalt eruptions at Pleiku and Buon Me Thuot, south-central Viet Nam, *J. Geodyn.*, *69*, 65–83, doi:10.1016/j.jog.2012.03.012.
- Huang, H., N. Tosi, S.-J. Chang, S. Xia, and X. Qiu (2015), Receiver function imaging of the mantle transition zone beneath the South China Block, *Geochem. Geophys. Geosyst.*, *16*, 3666–3678, doi:10.1002/2015GC005978.
- Huang, J. (2014), *P*- and *S*-wave tomography of the Hainan and surrounding regions: Insight into the Hainan plume, *Tectonophysics*, *633*, 176–192, doi:10.1016/j.tecto.2014.07.007.
- Huang, J., and D. Zhao (2006), High-resolution mantle tomography of China and surrounding regions, *J. Geophys. Res.*, *111*, B09305, doi:10.1029/2005JB004066.

- Huang, Z., D. Zhao, and L. Wang (2015), *P* wave tomography and anisotropy beneath Southeast Asia: Insight into mantle dynamics, *J. Geophys. Res.*, *120*, 5154–5174, doi:10.1002/2015JB012098.
- James, D. E., M. J. Fouch, R. W. Carlson, and J. B. Roth (2011), Slab fragmentation, edge flow and the origin of the Yellowstone hotspot track, *Earth Planet. Sci. Lett.*, *311*, 124–135.
- Langston, C. A. (1979), Structure under Mount Rainier, Washington, inferred from teleseismic body waves, *J. Geophys. Res.*, *84*, 4749–4762, doi:10.1029/JB084iB09p04749.
- Le, B. M., T. Yang, and S. Gu (2015), Upper mantle and transition zone structure beneath Leizhou-Hainan region: Seismic evidence for a lower-mantle origin of the Hainan plume, *J. Asian Earth Sci.*, *111*, 580–588, doi:10.1016/j.jseas.2015.06.008.
- Lei, J., D. Zhao, B. Steinberger, B. Wu, F. Shen, and Z. Li (2009), New seismic constraints on the upper mantle structure of the Hainan plume, *Phys. Earth Planet. Int.*, *173*, 33–50, doi:10.1016/j.pepi.2008.10.013.
- Leloup, P. H., R. Lacassin, P. Tapponnier, U. Scharer, D. Zhong, X. Liu, L. Zhang, S. Ji, and P. T. Trinh (1995), The Ailao Shan-Red River shear zone (Yunnan, China), Tertiary transform boundary of Indochina, *Tectonophysics*, *251*(1), 3–84, doi:10.1016/0040-1951(95)00070-4.
- Li, C., and R. D. van der Hilst (2010), Structure of the upper mantle and transition zone beneath Southeast Asia from traveltimes tomography, *J. Geophys. Res.*, *115*, B07308, doi:10.1029/2009JB006882.
- Li, C., R. D. van der Hilst, A. S. Meltzer, and E. R. Engdahl (2008), Subduction of the Indian lithosphere beneath the Tibetan Plateau and Burma, *Earth Planet. Sci. Lett.*, *274*, 157–168, doi:10.1016/j.epsl.2008.07.016.
- Litasov, K. D., E. Ohtani, A. Sano, A. Suzuki, and K. Funakoshi (2005), Wet subduction versus cold subduction, *Geophys. Res. Lett.*, *32*, L13312, doi:10.1029/2005GL022921.
- Liu, K. H., and S. S. Gao (2010), Spatial variations of crustal characteristics beneath the Hoggar swell, Algeria, revealed by systematic analyses of receiver functions from a single seismic station, *Geochem. Geophys. Geosyst.*, *11*, Q08011, doi:10.1029/2010GC003091.
- Montelli, R., G. Nolet, F. Dahlen, G. Masters, E. Engdahl, and S. Hung (2004), Finite-frequency tomography reveals a variety of plumes in the mantle, *Science*, *303*, 338–343, doi:10.1126/science.1092485.
- Pesicek, J. D., C. H. Thurber, S. Widiyantoro, E. R. Engdahl, and H. R. DeShon (2008), Complex slab subduction beneath northern Sumatra, *Geophys. Res. Lett.*, *35*, L20303, doi:10.1029/2008GL035262.
- Pesicek, J. D., C. H. Thurber, S. Widiyantoro, H. Zhang, H. R. DeShon, and E. R. Engdahl (2010), Sharpening the tomographic image of the subducting slab below Sumatra, the Andaman Islands and Burma, *Geophys. J. Int.*, *182*, 433–453, doi:10.1111/j.1365-246X.2010.04630.x.
- Ringwood, A. E. (1975), *Composition and Petrology of the Earth's Mantle*, 1st ed., 672 pp., McGraw-Hill, New York.
- Shearer, P. M., and M. P. Flanagan (1999), Seismic velocity and density jumps across the 410- and 660-kilometer discontinuities, *Science*, *285*, 1545–1548, doi:10.1126/science.285.5433.1545.
- Steckler, M. S., D. R. Mondal, S. H. Akhter, L. Seeber, L. Feng, J. Gale, E. M. Hill, and M. Howe (2016), Locked and loading megathrust linked to active subduction beneath the Indo-Burman Ranges, *Nat. Geosci.*, *9*(8), 615–618, doi:10.1038/ngeo2760.
- Takemoto, K., et al. (2009), Tectonic deformation of the Indochina Peninsula recorded in the Mesozoic palaeomagnetic results, *Geophys. J. Int.*, *179*(1), 97–111, doi:10.1111/j.1365-246X.2009.04274.x.
- Tang, Y., M. Obayashi, F. Niu, S. P. Grand, Y. J. Chen, H. Kawakatsu, S. Tanaka, J. Ning, and J. F. Ni (2014), Changbaishan volcanism in northeast China linked to subduction-induced mantle upwelling, *Nat. Geosci.*, *7*(6), 470–475, doi:10.1038/ngeo2166.
- Tapponnier, P., G. Peltzer, A. Y. Le Dain, R. Armijo, and P. Cobbold (1982), Propagating extrusion tectonics in Asia: New insights from simple experiments with plasticine, *Geology*, *10*, 611–616, doi:10.1130/0091-7613(1982)10<611:PETIAN>2.0.CO;2.
- Tapponnier, P., G. Peltzer, and R. Armijo (1986), On the mechanics of the collision between India and Asia, *Geol. Soc. Spec. Publ.*, *19*(1), 113–157, doi:10.1144/GSL.SP.1986.019.01.07.
- Tschauner, O., C. Ma, J. R. Beckett, C. Prescher, V. B. Prakapenka, and G. R. Rossman (2014), Discovery of bridgmanite, the most abundant mineral in Earth, in a shocked meteorite, *Science*, *346*(6213), 1100–1102, doi:10.1126/science.1259369.
- Wang, C.-Y., and J.-L. Huang (2012), Mantle transition zone structure around Hainan by receiver function analysis [in Chinese], *Chin. J. Geophys.*, *55*(4), 1161–1167, doi:10.6038/j.issn.0001-5733.2012.04.012.
- Wei, S. S., and Y. J. Chen (2016), Seismic evidence of the Hainan mantle plume by receiver function analysis in southern China, *Geophys. Res. Lett.*, *43*, 8978–8985, doi:10.1002/2016GL069513.
- Wood, B. J. (1995), The effect of H₂O on the 410-kilometer seismic discontinuity, *Science*, *268*, 74–76.
- Xia, S., D. Zhao, J. Sun, and H. Huang (2016), Teleseismic imaging of the mantle beneath southernmost China: New insights into the Hainan plume, *Gondwana Res.*, *36*, 46–56, doi:10.1016/j.gr.2016.05.003.
- Yang, T., F. Liu, N. Harmon, K. P. Le, S. Gu, and M. Xue (2015), Lithospheric structure beneath Indochina block from Rayleigh wave phase velocity tomography, *Geophys. J. Int.*, *200*(3), 1582–1595, doi:10.1093/gji/ggu488.
- Zhang, R., Y. Wu, Z. Gao, Y. V. Fu, L. Sun, Q. Wu, and Z. Ding (2017), Upper mantle discontinuity structure beneath eastern and southeastern Tibet: New constraints on the Tengchong intraplate volcano and signatures of detached lithosphere under the western Yangtze Craton, *J. Geophys. Res. Solid Earth*, *122*, 1367–1380, doi:10.1002/2016JB013551.
- Zou, H., and Q. Fan (2010), U-Th isotopes in Hainan basalts: Implications for sub-asthenospheric origin of EM2 mantle endmember and the dynamics of melting beneath Hainan Island, *Lithos*, *116*(1–2), 145–152, doi:10.1016/j.lithos.2010.01.010.